

# *Modeling of HDT pneumatic drying machine for moisture control*

Article

Published Version

Creative Commons: Attribution 4.0 (CC-BY)

Open Access

Zhu, X., Zhou, C., Su, H., Pan, F., Yang, K., Cao, Y. and Yang, S. ORCID: <https://orcid.org/0000-0003-0717-5009> (2025) Modeling of HDT pneumatic drying machine for moisture control. *Drying Technology*. ISSN 1532-2300 doi: 10.1080/07373937.2025.2481614 Available at <https://centaur.reading.ac.uk/122202/>

It is advisable to refer to the publisher's version if you intend to cite from the work. See [Guidance on citing](#).

To link to this article DOI: <http://dx.doi.org/10.1080/07373937.2025.2481614>

Publisher: Taylor and Francis

All outputs in CentAUR are protected by Intellectual Property Rights law, including copyright law. Copyright and IPR is retained by the creators or other copyright holders. Terms and conditions for use of this material are defined in the [End User Agreement](#).

[www.reading.ac.uk/centaur](http://www.reading.ac.uk/centaur)

**CentAUR**

Central Archive at the University of Reading

Reading's research outputs online



## Modeling of HDT pneumatic drying machine for moisture control

Xincheng Zhu, Chenchen Zhou, Hongxin Su, Fanda Pan, Kaihua Yang, Yi Cao & Shuanghua Yang

To cite this article: Xincheng Zhu, Chenchen Zhou, Hongxin Su, Fanda Pan, Kaihua Yang, Yi Cao & Shuanghua Yang (26 Mar 2025): Modeling of HDT pneumatic drying machine for moisture control, Drying Technology, DOI: [10.1080/07373937.2025.2481614](https://doi.org/10.1080/07373937.2025.2481614)

To link to this article: <https://doi.org/10.1080/07373937.2025.2481614>



© 2025 The Author(s). Published with license by Taylor & Francis Group, LLC



Published online: 26 Mar 2025.



Submit your article to this journal [↗](#)



Article views: 69



View related articles [↗](#)



View Crossmark data [↗](#)

## Modeling of HDT pneumatic drying machine for moisture control

Xincheng Zhu<sup>a</sup>, Chenchen Zhou<sup>a,b</sup>, Hongxin Su<sup>a</sup>, Fanda Pan<sup>c</sup>, Kaihua Yang<sup>c</sup>, Yi Cao<sup>a,b,d</sup>, and Shuanghua Yang<sup>a,b,d</sup>

<sup>a</sup>College of Chemical and Biological Engineering, Zhejiang University, Hangzhou, Zhejiang, China; <sup>b</sup>Institute of Zhejiang University-Quzhou, Quzhou, Zhejiang, China; <sup>c</sup>Technology Center, China Tobacco Zhejiang Industrial Co., Ltd, Hangzhou, Zhejiang, China; <sup>d</sup>Department of Computer Science, University of Reading, Reading, UK

### ABSTRACT

The drying process in cigarette factories, centered around the HDT pneumatic drying machine, has historically faced significant challenges with moisture inconsistency. To address this issue, a steady-state model grounded in mass and energy conservation principles was developed, focusing on key variables such as tobacco moisture content and temperature. By integrating model-based feedforward control, the system successfully reduced moisture fluctuations across different batches, ensuring more consistent tobacco moisture levels. Validation through Monte Carlo simulation confirmed the model's accuracy, and actual control effect demonstrated a mean reduction of 7.65% in the standard deviation of cooling moisture and a 20.27% decrease in the standard deviation of overall moisture variation, significantly improving batch consistency.

### ARTICLE HISTORY

Received 4 November 2024  
Revised 16 March 2025  
Accepted 16 March 2025

### KEYWORDS



HDT pneumatic drying process; process modeling; Monte Carlo simulation; tobacco moisture control

## 1. Introduction

In cigarette production, small fluctuations in tobacco moisture can significantly impact its aroma and taste, thus affected overall product quality,<sup>[1]</sup> which has attracted widespread attention from engineers. The HDT pneumatic drying machine (abbreviated as the HDT dryer) was invented to address the clumping issue by introducing high-temperature steam with anti-roping steam during startup and production phases, but the moisture consistency of the dried cut tobacco was poor. Specifically, the standard deviation of cooling moisture within a batch of cut tobacco was relatively large, with significant variability in the cooling moisture standard deviation across different batches. Therefore, it was of great necessity to implement better control strategy for the drying equipment to manage moisture fluctuations occurring during the production process. The HDT pneumatic drying process in a cigarette factory mainly included the HDT dryer, an outfeed conveyor and a winnower, and the original control structure was shown in the Figure 1.

In the Figure 1,  $X_{cool}$  represented the moisture content of tobacco after the drying, transportation, and

winnowing processes, while  $X_{cool}^{set}$  referred to the target value for  $X_{cool}$ , and  $u$  denoted the manipulated variables in the pneumatic drying process. The original control strategy for the HDT dryer relied on the deviation between  $X_{cool}$  and  $X_{cool}^{set}$  to control moisture fluctuations with a feedback controller in Figure 1. However, there was a significant time lag between moisture measurements at the inlet of the HDT dryer and the outlet of the winnower, preventing timely correction of disturbances. In actual production, the HDT dryer processed multiple grades of tobacco, each varying significantly in physical and chemical properties. This variation resulted in substantial differences in heat and mass transfer over short periods. But due to the lack of the comprehension of the process, engineers had to manually adjust equipment parameters based on experience, leading to inefficiencies and often resulting in large quantities of tobacco leaves being wasted, ultimately reducing profitability. In addition, the thin, long shape of individual tobacco strips, combined with high-temperature dry airflow, easily led to expansion, collisions, and entanglement with other strips, as well as contact with the walls of the accelerated bending arc. These factors introduced

**CONTACT** Shuanghua Yang  shuang-hua.yang@reading.ac.uk  College of Chemical and Biological Engineering, Zhejiang University, Hangzhou, Zhejiang, China

© 2025 The Author(s). Published with license by Taylor & Francis Group, LLC

This is an Open Access article distributed under the terms of the Creative Commons Attribution License (<http://creativecommons.org/licenses/by/4.0/>), which permits unrestricted use, distribution, and reproduction in any medium, provided the original work is properly cited. The terms on which this article has been published allow the posting of the Accepted Manuscript in a repository by the author(s) or with their consent.

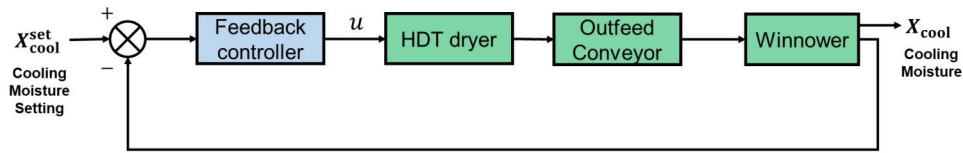


**Figure 1.** The original cooling water feedback control system structure of the cigarette factory.

random effects into the drying process. Moisture inconsistency at the inlet of the HDT dryer, the unpredictability of motion, and the randomness in heat and mass transfer in the accelerated bending arc contributed to the fluctuation in the moisture content of tobacco after drying. In short, such control strategy based on the feedback controller was impossible to meet the requirement of multiple sources of disturbances.

The dryer was the core equipment in the drying process, and enhancing its control over random disturbances held significant industrial value. Various control strategies had been applied to drying processes, including internal model control,<sup>[2]</sup> fuzzy control,<sup>[3]</sup> and model predictive control.<sup>[4,5]</sup> Building on existing PID control algorithms, Bi et al.<sup>[6]</sup> proposed a new intelligent actor-critic control system that utilized reinforcement learning to optimize the dynamic configuration of rotary dryers. Wu et al.<sup>[7]</sup> employed an accumulated temperature mathematical model, derived from experimental data and implemented in software, for the automatic control of continuous drying processes. However, this control strategy relied on extensive sensing devices, which was not feasible for HDT pneumatic drying process. Li et al.<sup>[8]</sup> introduced a recurrent self-evolving fuzzy neural network predictive control scheme to determine suitable input power over a prediction horizon. Bahareh et al.<sup>[9]</sup> utilized machine vision techniques to determine color and shrinkage as qualitative indicators and developed artificial neural network models for predicting drying variables in a laboratory-scale fluidized bed shelled corn dryer. Nevertheless, managing tobacco with significant property differences often required accumulating substantial experimental data and incurring high costs for model development and training. To eliminate moisture fluctuations caused by unknown stochastic sources, it was essential to identify the primary influencing factors and understand how they impacted the state variables of tobacco. In practice, numerous factors could affect tobacco moisture content during the drying process,<sup>[10]</sup> including moisture distribution at the dryer inlet, morphological characteristics, and the humidity and temperature of the process gas. From the perspective of the first principle, classical theories such as the two-fluid theory<sup>[11-13]</sup> and the Eulerian granular method<sup>[14,15]</sup> were widely used in the drying

process. By applying the continuum medium model, modeling considered granulates as a pseudo-fluid and solved motion equations for particles and fluids within the Eulerian coordinate system to obtain detailed information about particle motion. Levy A. et al.<sup>[16]</sup> developed a reliable model based on two-fluid theory to predict moisture content during the drying process of wet PVC particles in a pneumatic dryer. However, unlike small laboratory-scale dryers, industrial dryers were much larger, and the internal conditions of the materials were not easily observable. The primary challenges in studying drying processes were well-recognized, including their nonlinearity, unknown dynamics, and the coupling of heat, mass, and momentum transfer.<sup>[17]</sup> Additionally, there was a lack of sufficient detection equipment to gather necessary measurement data for calculating relevant parameters and understanding the states of process gas and materials. Consequently, conducting in-depth research on randomness and establishing a mechanism model capable of accurately predicting material states during drying was extremely challenging. To date, there have been few studies on moisture control in pneumatic drying machines, particularly the HDT dryers, and limited work on modeling the entire process.

To improve the control of tobacco's cooling moisture, this paper developed a steady-state model of the HDT drying process based on first principles, which would be able to provide a robust theoretical foundation for improving control strategies. The model identified stochastic sources affecting cooling moisture and explained their impacts mechanistically. Based on these insights, a feedforward control strategy was implemented to reduce fluctuations in cooling moisture and variability in moisture content across batches. The study relied on mass and energy conservation principles, with tobacco moisture content and temperature as key state variables for the model's state equations. In the HDT dryer section, tobacco leaves were modeled as cylindrical particles, revealing that moisture content at the dryer inlet and the characteristic length of the tobacco leaves were major sources of moisture fluctuations. A layered model for the outfeed conveyor section was developed using Fick's second law, while a mixer model for the winnower section accounted for mixing and averaging effects.

The model would be beneficial for solving the problem of time lag by predicting output state based on input data. Integrating the feedforward control strategy with the existing feedback control system in the cigarette factory effectively reduced moisture fluctuations and enhanced overall drying quality.

The rest of the paper was following: in Section 2, a brief introduction to HDT drying process was provided, including the division of the process sections, measurement conditions, and the selection of key process variables; in Section 3, modeling for the HDT drying machine section, the outfeed conveyor section, and the winnower section were established sequentially. Following this, the parameter optimization problem was discussed. The model was validated using Monte Carlo methods in Section 4. And in Section 5, the feedforward control strategy based on the steady-state model was introduced, and this model was integrated with the improved control strategy and tested in practical applications. Finally, Section 6 concluded the paper.

## 2. HDT pneumatic drying process and key process variables

### 2.1. HDT pneumatic drying process

HDT pneumatic drying process scene in the cigarette factory was shown in Figure 2.

Tobacco moved from left to right through various devices, sequentially undergoing drying, transmission, and winnowing processes. Based on the characteristics of these equipments and changes in the state of the tobacco, the entire process was divided into three sections: the HDT dryer section, the outfeed conveyor section and the winnower section.

The HDT dryer section consisted of a distance on the conveyor and the HDT dryer and the loss of moisture from tobacco on the infeed conveyor was

not considered. Inside the dryer, tobacco strips dropped into the accelerated bending arc while coming into contact with anti-roping steam, which caused tobacco strips to quickly warm up and expand. As the tobacco entered the accelerated bending arc, heat exchange led to rapid moisture evaporation and a sharp rise in temperature. An infrared moisture meter was installed on the conveyor at the dryer outlet, allowing real-time detection of the tobacco's moisture content and temperature.

The outfeed conveyor section began at the moisture meter located at the start of the conveyor and ended at the inlet of the winnower. Along this section, the conveyor transported tobacco strips at a constant speed, allowing their temperature to gradually cool in a relatively stable environment. The conveying process took approximately 45 s for each piece of tobacco. No control interventions were applied during this stage, and heat and mass transfer occurred between the tobacco and the surrounding air in the workshop, along with minor internal mass and energy migration within the tobacco.

The winnower section mainly consisted of the winnower itself, with the distance between its outlet and the cooling moisture meter being negligible. Upon entering this section, the tobacco was subjected to a strong airflow that separated the strips, tossing and mixing them for approximately 9 s before leaving. At the winnower's outlet, the tobacco's moisture content was measured by the cooling moisture meter before being transported to the next stage of the production process.

### 2.2. Measuring instruments and sampling conditions

Measuring instruments in the HDT pneumatic drying process primarily included belt scales, infrared moisture meters, as well as detection probes and flow meters inside the dryer, which were not visible.

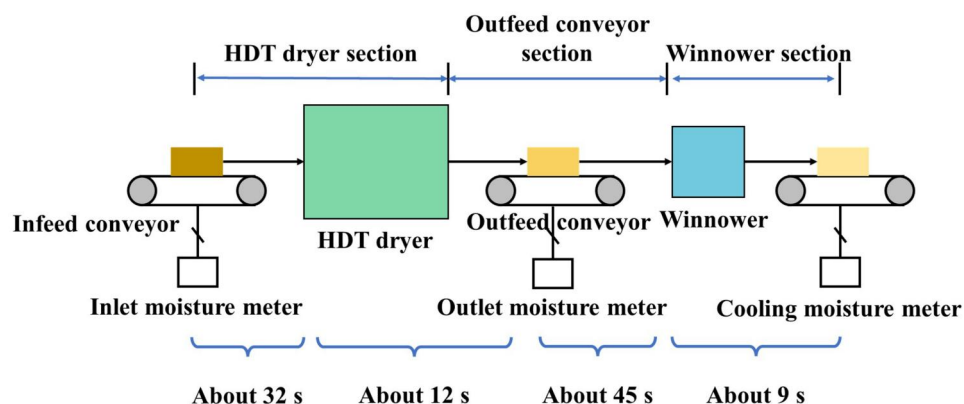


Figure 2. HDT pneumatic drying process.

Before the tobacco entered the HDT dryer, it passed over a weigh scale. Throughout the whole process, only this weigh scale at the entrance was used to measure and record the mass flow of the tobacco with a sensitivity of  $\pm 0.001 \text{ kg}$  and a range of 0 to 5000  $\text{kg/h}$ . And the moisture content of the tobacco was measured by three infrared moisture meters, each with a sampling area of 60 mm in circumferential block. The moisture content accuracy of the meter was  $\pm 0.1\%$ , with a range of 0 to 50%, and their temperature sensitivity was  $\pm 0.1 \text{ K}$ , with a range of 263 to 353  $\text{K}$ . These three infrared moisture meters were installed at the inlet and outlet of the HDT dryer and at the outlet of the winnower. The meter located at the dryer's inlet measured and recorded the inlet moisture of the tobacco; the one situated behind the dryer outlet measured and recorded both the moisture and temperature of the tobacco; and the meter near the winnower outlet measured the moisture and temperature of the tobacco but only recorded the moisture data. The flow meter inside the HDT dryer measured the volume flow of gas with a sensitivity of  $\pm 0.001 \text{ m}^3/\text{s}$  and a range of 0 to 10  $\text{m}^3/\text{s}$ . A temperature probe inside the HDT dryer was used to measure the temperature of the process gas, with a sensitivity of  $\pm 0.1 \text{ K}$  and a range of 273 to 473  $\text{K}$ . All these instruments recorded measurements once per second.

In order to verify whether the time series data obtained from the moisture meter were representative or not, an FLIR thermal camera was used to observe the temperature field in the detection area of the moisture meter at the outlet of the HDT dryer, and the range of temperature observed with this camera was 253.15 to 393.15  $\text{K}$ . The thermal imaging camera was placed above the moisture meter to observe the distribution of the temperature field of the tobacco (as shown in Figure 3) at different time, the brighter the color of an area, the higher the temperature. The color difference stood for temperature difference, and the temperature field was not evenly distributed, the temperature difference between the brightest and darkest areas in the image was as high as about 10  $\text{K}$ . In short, due to the small measurement area, the measurement data lacked representativeness.

### 2.3. Selection of key process variables

As previously noted, there was currently no control system designed for tobacco's states in the post-drying stages (the outfeed conveyor section and the winnower section), and the moisture content at the outlet of the HDT dryer, which was one of the initial states in the

post-drying stages, had a significant impact on cooling moisture. Therefore, it should be regarded as a critical process variable. During the drying process, the interaction between high-temperature gas and the tobacco facilitated heat transfer to the tobacco, indicating that the mass transfer process was accompanied by heat transfer, and thus both the outlet temperature of the dryer ( $T_{HDT}$ ) and the temperature of the hot air ( $T_{hot}$ ) were essential process variables. As the fundamental of mass conservation, the mass flow rate ( $F_{t, inlet}$ ) and moisture content of the tobacco at the dryer inlet ( $X_{inlet}$ ) were crucial input variables for the entire drying process. The raw process data did not include measurements of part of key variables for tobacco strips, such as density, specific heat, and moisture activity. For example, the drying process primarily occurred in the accelerated arc, but there were no measurements of gas humidity ( $H$ ) inside the duct, made it challenging to assess changes in the mass, energy, and momentum of the process gas after it interacted with tobacco strips. To cope with this problem, the values of some variables were derived from existing studies and adjusted using observable state variables, while others were estimated based on scientific judgment and used at fixed values in the model. The specifics of the modeling-related elements will be discussed in next section.

In the outfeed conveyor section, tobacco was exposed to ambient air for an extended period, and thus ambient temperature ( $T_{air}$ ) and relative humidity ( $RH$ ) were assumed to be time-invariant and treated at fixed values in the model. To assess moisture and temperature changes in the tobacco during its transit on the outfeed conveyor, a backup moisture meter was temporarily installed before the winnower inlet, and these two variables were denoted as  $X_{Conveyor}$  and  $T_{Conveyor}$ .

In the winnower section, historical data on operating process variables were lacking, with only cooling moisture data collected by the moisture meter at the winnower outlet. Routine production did not involve monitoring the cooling temperature, so this data was not recorded. In the aforementioned experiment, data on the winnower outlet temperature (cooling temperature, denoted as  $T_{cool}$ ) for the same batch of tobacco was obtained and considered as a key process variable. These additional measurements obtained would serve as crucial reference values for predicting unobserved tobacco states in the subsequent steady-state modeling and Monte Carlo simulations.

In summary, the final selected key process variables were shown in Table 1.



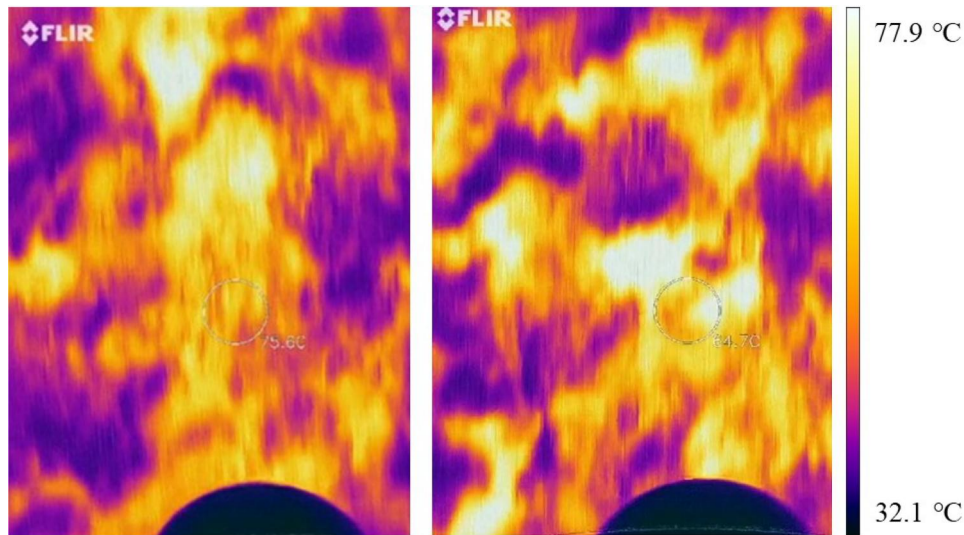


**Figure 3.** Scenes observed by FLIR thermal camera at two different times in a batch.

**Table 1.** Key process variables of HDT pneumatic drying process.

Key process variables	Symbol notation	Unit
Tobacco mass flow rate	$F_{t, inlet}$	kg/s
Moisture content at the inlet of the HDT dryer	$X_{inlet}$	–
Volume flow rate of process gas	$V_{pg}$	m <sup>3</sup> /s
Density of process gas	$\rho_{pg}$	kg/m <sup>3</sup>
Temperature of hot wind	$T_{hot}$	K
Moisture content at the outlet of the HDT dryer	$X_{HDT}$	–
Temperature at the outlet of the HDT dryer	$T_{HDT}$	K
Moisture content at the inlet of winnower	$X_{conveyor}$	–
Temperature at the inlet of winnower	$T_{conveyor}$	K
Cooling moisture content	$X_{cool}$	–
Cooling temperature	$T_{cool}$	K

### 3. Modeling and simulation on HDT pneumatic drying process

Steady-state modeling served as the foundation for studying HDT pneumatic drying process, capturing the steady-state behavior of industrial systems through mathematical methods. By constructing a mechanistic-based steady-state model, this approach allowed for a deep analysis of the change in tobacco moisture content and temperature during the drying process. This model provided a robust theoretical basis for optimizing control strategies in subsequent stages.

#### 3.1. Mechanistic equations for the HDT pneumatic drying process

##### 3.1.1. The HDT dryer section

In the HDT dryer section, tobacco was first transported to the dryer by the feed conveyor. It fell to the bottom of the accelerating arc, then rapidly rose to the top under the influence of high-temperature, high-speed airflow. The tobacco then entered a cyclone separator before finally falling onto the conveyor

at the dryer's outlet. This entire process primarily served to dry cut tobacco and separate gas from solids. The cyclone separator, an ideal gas-solid separator, and the accelerating arc together concentrated the drying process, with the accelerating arc being modeled as the dryer.

In the conservation of mass and energy, the mass loss of tobacco was primarily due to water evaporation. The change in energy was mainly attributed to the heat from evaporation and the convection heat transferred by the process gas. The incremental mass of tobacco inside the HDT dryer per unit time was denoted as  $\Delta m_{HDT}$  (kg); the incremental heat of tobacco was denoted as  $\Delta E_{HDT}$  (kJ); the evaporation of water from tobacco was denoted as  $Evap_{HDT}$  (kg); the enthalpy flow of tobacco at the dryer entrance was denoted as  $h_{t, HDT, in}$  (kJ/s); the heat removed by the evaporation of moisture from tobacco was denoted as  $Q_{evap, HDT}$  (kJ); and the heat transferred to the tobacco by the process gas was denoted as  $Q_{conv, HDT}$  (kJ). Taking the tobacco inside the drying machine as the subject, the following equation was established based on the conservation of mass and energy:

$$\begin{cases} \Delta m_{HDT} = F_{t, inlet} \Delta t - F_{t, HDT, out} \Delta t - Evap_{HDT} \\ \Delta E_{HDT} = h_{t, HDT, in} \Delta t - h_{t, HDT, out} \Delta t - Q_{evap, HDT} - Q_{conv, HDT} \end{cases} \quad (1)$$

where  $F_{t, HDT, out}$  represented the mass flow rate of tobacco at the outlet of the HDT dryer, kg/s; and  $h_{t, HDT, out}$  denoted the enthalpy flow rate of tobacco at the dryer outlet, kJ/s. Due to the lack of measuring devices in the accelerated bending arc of the HDT dryer, it was not possible to monitor the changes in the gas state during its interaction with the tobacco.



Given the high flow rate of the process gas (ranging from 5.200 to 5.300  $m^3/s$ ), its mass flow was between 2.650 and 2.750  $kg/s$ , which was approximately twice the mass flow of the tobacco (about 1.250  $kg/s$ ). Therefore, the process gas was assumed to have constant temperature, humidity and a stable flow rate.  $h_{t,HDT,in}$  and  $h_{t,HDT,out}$  represented the enthalpy flow rate of tobacco entering and leaving the dryer, in  $kJ/s$ , and it can be calculated as shown in Equation 2:

$$\begin{cases} h_{t,HDT,in} = C_{p,in} F_{inlet} T_{inlet} \\ h_{t,HDT,out} = C_{p,out} F_{t,HDT,out} T_{t,HDT,out} \end{cases} \quad (2)$$

$C_p$  represented the specific heat capacity of tobacco, with  $C_{p,in}$  and  $C_{p,out}$  denoting the specific heat at the dryer's inlet and outlet, respectively, both measured in  $kJ/(kg K)$ .  $T_t$  indicated the temperature of the tobacco, while  $T_{inlet}$  referred to the temperature of the tobacco at the dryer's inlet, measured in Kelvin. Without considering chemical changes and assuming that tobacco consisted solely of dry matter and moisture, the mass flow of dry tobacco remained constant across different devices, with only the moisture content varying. Based on Equation 3, the values of  $F_{inlet}$  and  $X_{in}$  can be calculated from the absolute dry tobacco mass flow,  $F_{t,dry}$ .

$$F_{t,HDT,in} = F_{t,dry}(1 + X_{inlet}) \quad (3)$$

$C_p$  was obtained using Equation 4 fitting:

$$C_p = \theta_{C_{p1}} + \theta_{C_{p2}} X \quad (4)$$

where  $\theta_{C_{p1}}$  and  $\theta_{C_{p2}}$  were considered as model parameters, and the fitting result was shown in the Table 2.

To calculate  $Evap_{HDT}$ ,  $Q_{evap,HDT}$ , and  $Q_{conv,HDT}$ , it was required to determine the evaporation or heat transfer area based on the shape of the object under study during the drying process. As for the shape of tobacco inside HDT deryer, on the one hand, the shape of tobacco was slender and elongated, with very small bottom areas at both ends and large side areas. When tobacco got heated and expanded, it was easy to entangle together. On the other hand, tobacco had the characteristic of varying lengths, which meant the surface area (contact area) of different tobacco was different. Based on the above facts, it was reasonable to consider modeling tobacco as cylindrical particles—all with the same base area and different lengths, remained constant throughout the drying process. The calculation was as followed:

$$A_{HDT} = 2\pi r^2 + 2\pi r L_t \quad (5)$$

where  $r$  denoted the radius of the base of the cylinder, and  $L_t$  denoted the characteristic length of the tobacco particles.

**Table 2.** The result of fitting model parameters.

Model parameters	Value	Model parameters	Value
$k_{HDT}$	$1.000 \times 10^{-1}$	$\lambda_7$	5
$h_{HDT}$	$1.000 \times 10^{-3}$	$\lambda_8$	1
$r$	$9.369 \times 10^{-3}$	$\lambda_9$	1
$\theta_{C_{p1}}$	3	$\lambda_{10}$	4
$\theta_{C_{p2}}$	5	$\lambda_{11}$	1
$\theta_{\rho_1}$	$5.540 \times 10^1$	$\lambda_{12}$	5
$\theta_{\rho_2}$	$-2.259 \times 10^1$	$\Theta_{Xe1}$	$2.851 \times 10^{-1}$
$\theta_{\rho_3}$	1	$\Theta_{Xe2}$	$-5.500 \times 10^{-4}$
$\theta_{\rho_4}$	$-1.359 \times 10^2$	$\Theta_{Xe3}$	$9.000 \times 10^{-1}$
$\theta_{\rho_5}$	$5.260 \times 10^2$	$B_1$	$4.936 \times 10^{-5}$
$\theta_{\rho_6}$	$-3.443 \times 10^1$	$B_2$	$-2.030 \times 10^{-2}$
$\theta_{aw1}$	$-2.512 \times 10^7$	$Ea$	$2.426 \times 10^1$
$\theta_{aw2}$	-8.209	$RH$	$5.483 \times 10^1$
$\theta_{aw3}$	$-4.764 \times 10^{-1}$	$k$	$5.000 \times 10^{-2}$
$\theta_{aw4}$	4	$h_{conveyor}$	$9.896 \times 10^{-3}$
$L_t$	$4.079 \times 10^{-2}$	$h_{winnow}$	$5.762 \times 10^{-1}$
$\lambda_1$	4	$m_{winnow}$	$5.000 \times 10^{-2}$
$\lambda_2$	3	$X_{winnow}$	$1.365 \times 10^{-1}$
$\lambda_3$	4	$T_{winnow}$	$3.010 \times 10^2$
$\lambda_4$	1	$\Theta_{R1}$	$1.637 \times 10^{-1}$
$\lambda_5$	3	$\Theta_{R2}$	$3.549 \times 10^{-7}$
$\lambda_6$	3	$\Theta_{R3}$	1

The convective heat transfer between the tobacco particles and the air stream was calculated using Equation 6:

$$Q_{conv,HDT} = h_{HDT} A_{HDT} (T_t - T_g) \quad (6)$$

where  $h_{HDT}$  represented the heat transfer coefficient, in  $kJ/(m^2 K)$ .  $A_{HDT}$  was the outer surface area of the tobacco,  $T_t$  was the temperature of the tobacco particles, and  $T_g$  donated as the temperature of hot air. The fitting result of coefficients was listed in the Table 2.

Tanaka et al.,<sup>[18]</sup> based on the thermodynamic properties of gas-vapor mixtures, proposed that the driving force for the evaporation process was the difference between the surface's saturated humidity and the humidity of the gas. Their proposed evaporation formula was as followed:

$$W = k_{HDT} \left[ 0.622 \frac{a_w P_{sat}(T_t)}{P - a_w P_{sat}(T_t)} - H \right] \quad (7)$$

In this equation,  $k_{HDT}$  was the model coefficient,  $P$  was the gas pressure,  $a_w$  was the moisture activity,  $P_{sat}(T_t)$  was the saturated vapor pressure at temperature  $T_t$ , and  $H$  was the absolute humidity of the gas. Due to the lack of direct measurements of the process gas humidity.

$Q_{evap,HDT}$  in the Equation 1 can be calculated as below:

$$Q_{evap,HDT} = Evap_{HDT} L(T_t, X) \quad (8)$$

In the equation above,  $L(T_t, X)$  was the latent heat of evaporation, unit was  $kJ/kg$ . According to the report of Murata et al.,<sup>[19]</sup>  $L(T_t, X)$  can be calculated as Equations 9–12:

$$L(T_t, X) = (V_v - V_l)T_t \left( \frac{dP_t(T_t, X)}{dT_t} \right)_V \quad (9)$$

$$V_v - V_l = \frac{461.5T_t}{P_t(T_t, X)} - 0.001 \quad (10)$$

$$P_t(T_t, X) = a_w(T_t, X)P_{sat}(T_t) \quad (11)$$

$$\left( \frac{dP_t(T_t, X)}{dT_t} \right)_V = \left( \frac{da_w(T_t, X)}{dT_t} \right)_V P_{sat}(T_t) + a_w(T_t, X) \left( \frac{dP_{sat}(T_t)}{dT_t} \right)_V \quad (12)$$

where  $V_v$  and  $V_l$  represented the volume of vapor and liquid, respectively,  $P_t$  denoted as the pressure of tobacco's water, and  $a_w$  was water's activity.

In actual drying process, the temperature and moisture of tobacco varied continuously, making the precise calculation of  $Evap_{HDT}$ ,  $Q_{evap, HDT}$ , and  $Q_{conv, HDT}$  complex, as it involved double integration. The estimated state was the upper limit of this integration, which complicated the solution process. To simplify this, the integral median theorem was applied, using median values for moisture and temperature in the calculations of  $Evap_{HDT}$ ,  $Q_{evap, HDT}$ , and  $Q_{conv, HDT}$ . In Equations 13 and 14, the median values for tobacco moisture and temperature in the HDT dryer section were approximated by introducing four model parameters ( $\lambda_1$ ,  $\lambda_2$ ,  $\lambda_3$ , and  $\lambda_4$ ):

$$X_{HDT, mid} = \frac{\lambda_1 X_{inlet} + \lambda_2 X_{HDT}}{\lambda_1 + \lambda_2} \quad (13)$$

$$T_{HDT, mid} = \frac{\lambda_3 T_{inlet} + \lambda_4 T_{HDT}}{\lambda_3 + \lambda_4} \quad (14)$$

In view of the mathematical model of rice powder developed by Tanaka et al.,<sup>[18]</sup> Equation 15 was used to associate  $\rho_t$  with T and X, and Equation 16 was used to associate  $a_w$  with  $T_t$  and X. The equation was used to calculate  $P_{sat}$ :

$$\rho_t = \exp(\theta_{\rho_1} X^2 + \theta_{\rho_2} X + \theta_{\rho_3}) \quad (15)$$

$$a_w = \exp(\theta_{aw1} T_t^{\theta_{aw2}} \exp(\theta_{aw3} T_t^{\theta_{aw4}} X)) \quad (16)$$

where  $\theta_{\rho_1}$ ,  $\theta_{\rho_2}$ ,  $\theta_{\rho_3}$ ,  $\theta_{\rho_4}$ ,  $\theta_{\rho_5}$ ,  $\theta_{\rho_6}$ ,  $\theta_{aw2}$ ,  $\theta_{aw3}$ ,  $\theta_{aw4}$  were model parameters.

In the mechanistic equations for the HDT dryer section, both  $k_{HDT}$  and  $h_{HDT}$  were used as model parameters without incorporating more detailed, specific calculation formulas. Meanwhile,  $A_{HDT}$  influenced both heat and mass transfer calculations. With  $r$  as a fixed parameter, the characteristic length of the tobacco,  $L_t$ , served as the sole variable factor. Observations at the conveyor feeding into the dryer revealed that the tobacco strips were unevenly

distributed in length, and were prone to clumping together, with some already forming into lumps. This clumping resulted in uneven heat and mass transfer, leading to significant fluctuations in the tobacco's moisture content post-drying. In the mathematical model, variations in  $L_t$  affected the contact area between the tobacco and the gas, impacting heat and mass transfer calculations and introducing randomness into the drying process. Aside from this, the calculation of  $a_w$ ,  $C_p$ , and  $\rho_t$  were related to moisture content. Additionally, fluctuations in  $X_{inlet}$ , as an input variable to the model, significantly impacted the stability of moisture levels after drying (Figure 4).

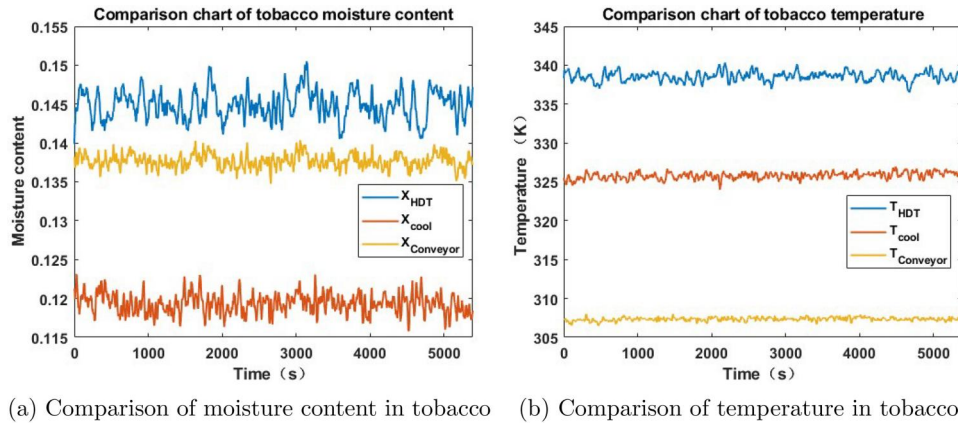
### 3.1.2. Outfeed conveyor section

Tobacco was steadily transported on the outfeed conveyor section, where extended exposure of the surface to ambient air resulted in greater dissipation of moisture and heat compared to the internal diffusion within the tobacco. To better understand the moisture and temperature differences between the surface and internal tobacco shreds, an additional infrared moisture meter was temporarily installed in front of the winnower to measure  $X_{Conveyor}$  and  $T_{Conveyor}$  in real time. Data on  $T_{cool}$  from the cooling moisture meter was also collected during the test. The comparison of moisture content and temperature of tobacco in the post-drying process was shown in the Figure 5.

By analyzing the 5390-second measurements from the special experimental batch in the Figure 5a, it was found that  $X_{HDT}$  had the highest mean value of 0.1449, while  $X_{Conveyor}$  had a mean of 0.1193, significantly lower than  $X_{cool}$ , which had a mean of 0.1337. In the Figure 5b, the temperature  $T_{HDT}$  exhibited the



Figure 4. Agglomerated tobacco at the entrance of the dryer.



(a) Comparison of moisture content in tobacco (b) Comparison of temperature in tobacco

**Figure 5.** Comparison of moisture content and temperature of tobacco in the post-drying process.

highest mean value of 338.6 K, followed by the temperature before the inlet of the winnower at 325.8 K, and  $T_{cool}$  at 307.3 K. The pressure inside the winnower was lower than the ambient air pressure. Therefore, it was difficult for tobacco, whose moisture content was higher than the equilibrium moisture<sup>[19]</sup> to absorb moisture in a negative pressure environment, and it was reasonable to believe the increase in moisture content of tobacco as it left the winnower was likely due to the obvious mixing effect during the winnowing process.

According to the the result of the experiment, it suggested that a significant amount of moisture was lost from the upper layer of the tobacco shred in the outfeed conveyor section, and the evaporation process there could not be disregarded. Additionally, the large difference between  $X_{Conveyor}$  and  $X_{cool}$  implied that moisture reduction was greater on the surface of the tobacco in the outfeed conveyor section compared to the internal layers, and the winnower effectively mixed the upper and lower layers of tobacco. Therefore, it was crucial to distinguish between the internal and external layers of tobacco in the outfeed conveyor section.

Different from the HDT dryer section where tobacco was blown into strips and came into full contact with process gas, tobacco piled up together in this section and then steadily moves to the entrance of the winnower, and its surface tobacco had a larger contact area with the air, which would diffuse more moisture and heat, and thus the shape that tobacco in this section was considered into rectangular. Here, tobacco was divided into upper and lower layers as shown in the Figure 6. All evaporation and heat dissipation occurred in the upper layer, while the lower layer remained unchanged, without transferring energy or diffusing moisture to the upper layer. Let  $k$  represent the ratio of the upper layer's dry tobacco mass flow to

$F_{t,dry}$ ; thus, the lower layer's dry tobacco mass flow accounted for  $1-k$ . The calculation formula was shown in Equation 17.

$$\begin{aligned} F_{t,HDT,out} &= F_{t,Conveyor,in} \\ &= kF_{t,dry}(1 + X_{HDT}) + (1 - k)F_{t,dry}(1 + X_{HDT}) \end{aligned} \quad (17)$$

$$\frac{\partial X}{\partial t} = D_{eff} \frac{\partial^2 X}{\partial x^2} \quad (18)$$

Fick's law of diffusion (Equation 18) was a classical law describing the diffusion behavior of substances in a medium. In the process of moisture diffusion from the tobacco to the air ( $x$  denoted the diffusion distance in m),  $D_{eff}$  was the effective diffusion coefficient.

$$MR = \frac{X - X_e}{X_0 - X_e} \quad (19)$$

MR in Equation 19 denoted the moisture ratio,  $X$  denoted the moisture after drying,  $X_e$  represented the equilibrium moisture, and  $X_0$  was the initial moisture. To solve the equation, Crank assumed that external resistance to mass transfer was negligible, the initial humidity and temperature were uniform, and material shrinkage was minimal.<sup>[20]</sup> The moisture diffusion equation for the outfeed conveyor was as follows:

$$MR = \frac{8}{\pi^2} \sum_{n=1}^N \frac{1}{(2n-1)^2} \exp\left(-\frac{(2n-1)^2 \pi^2 D_{eff} t_{Conveyor}}{L_{thick}^2}\right) \quad (20)$$

Here,  $t_{Conveyor}$  denoted the time experienced by moisture diffusion, which approximated the time the tobacco spends on the outfeed conveyor.  $L_{thick}$  represented the diffusion path, was approximate to half of the thickness of the tobacco, all measured in m. Based on Equation 20,  $X_{Conveyor}$  can be calculated.

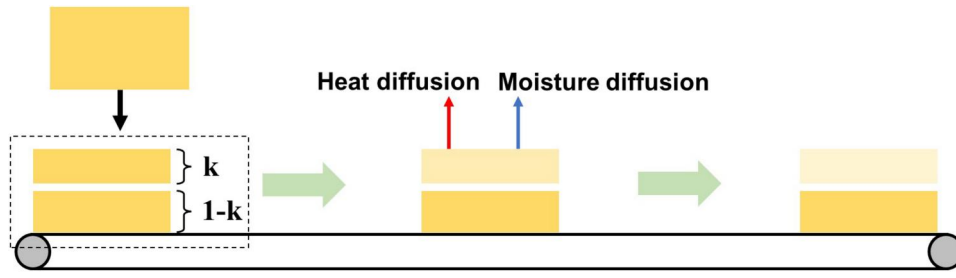


**Figure 6.** Schematic diagram of the layered model of the outfeed conveyor section.

$X_e$  in the Equation 19 can be calculated by applying Modified Oswin Model.<sup>[21]</sup>

$$Xe = (\theta_{Xe1} + \theta_{Xe2}T) \left( \frac{RH/100}{1-RH/100} \right)^{\theta_{Xe3}} \quad (21)$$

$D_{eff}$  would be affected by environmental factors such as the temperature of the workshop and the relative humidity of the air ( $RH$ ). It can be computed by the equation below<sup>[19]</sup>

$$D_{eff} = B_1 \exp\left(-\frac{E_a}{RT} + B_2 \frac{RH}{100}\right) \quad (22)$$

Both  $B_1$  and  $B_2$  were parameters. Due to the unknown relative humidity of the air near the conveyor,  $RH$  can only be estimated based on the approximate relative humidity within the workshop, treated as a model parameter. For the upper layer of tobacco, the heat transfer equation was referenced in Equation 24. The tobacco on the outfeed conveyor was approximated as a rectangular shape, and its width and height were estimated to determine the heat transfer area (conveying speed  $v_{Conveyor}$  was 0.6333 m/s, the width was 0.4 m), and the heat transfer coefficient,  $h_{Conveyor}$  was treated as a model parameter. The enthalpy flow  $h_{t,Conveyor,in}$  at the starting position of the tobacco outfeed conveyor was  $h_{t,HDT,in}$ , and the energy increment of the tobacco at this stage was expressed as followed:

$$\Delta E_{t,Conveyor} = h_{t,Conveyor,in} \Delta t - h_{t,Conveyor,out} \Delta t - Q_{Conveyor,conv} - Q_{Conveyor,evap} \quad (23)$$

$$Q_{Conveyor,conv} = h_{Conveyor} (v_{Conveyor} \times 0.4 + v_{Conveyor} \times *L_{thick} * 2) \Delta t (T - T_{air}) \quad (24)$$

$\Delta t$  denoted the tobacco's time in this section, and  $T_{air}$  denoted the temperature of the ambient air. There was no measurement device in the winnower, since the air pressure inside the winnower was low, the ambient air would be drawn in. Therefore, the gas temperature inside the winnower was assumed to be the same as the ambient temperature, 298.15 K. To

calculate  $Q_{evap,Conveyor}$ , it was prior to calculate the moisture evaporation mass ( $Evap_{Conveyor}$ ) during this stage, and then multiplied it by  $L(T_t, X)$ . Based on the assumption, the evaporation of water was all concentrated in the upper layer of the tobacco, and thus the value of  $Evap_{Conveyor}$  can be calculated as follows:

$$Evap_{Conveyor} = kF_{t,dry} \Delta t (X_{HDT} - X_{Conveyor}) \quad (25)$$

To simplify double integration of  $Q_{evap,HDT}$  and  $Q_{conv,HDT}$ , the integral median theorem was employed, introducing four model parameters ( $\lambda_5, \lambda_6, \lambda_7, \lambda_8$ ) to estimate state medians.

$$X_{Conveyor,mid} = \frac{\lambda_5 X_{HDT} + \lambda_6 X_{Conveyor}}{\lambda_5 + \lambda_6} \quad (26)$$

$$T_{Conveyor,mid} = \frac{\lambda_7 T_{HDT} + \lambda_8 T_{Conveyor}}{\lambda_7 + \lambda_8} \quad (27)$$

### 3.1.3. Winnower section

In the winnower section, the tobacco that was originally piled on the conveyor was blown into strips by strong wind after entering the winnower, and then churned in a closed space. During the winnowing process, the newly entered tobacco mixed with the tobacco already inside, and then settled into the outlet channel of the winnower before leaving the device. There was no heat source or measuring device in the winnower, and the equipment parameters remained constant. In this process, due to evaporation, tobacco lost moisture and heat, but achieved a certain degree of moisture and heat mixing between each other. Besides, the convective heat transfer between the strong airflow and tobacco also caused significant heat loss. After this process, the temperature of the tobacco rapidly decreased, and the fluctuation in tobacco moisture decreased apparently.

The schematic diagram of the entire mixing process was shown in Figure 7.

It was advisable to model the winnower as a mixer: some tobacco always stayed in the mixer (B tobacco was one of them), and the moisture content of B tobacco was lower than that of the lower layer of



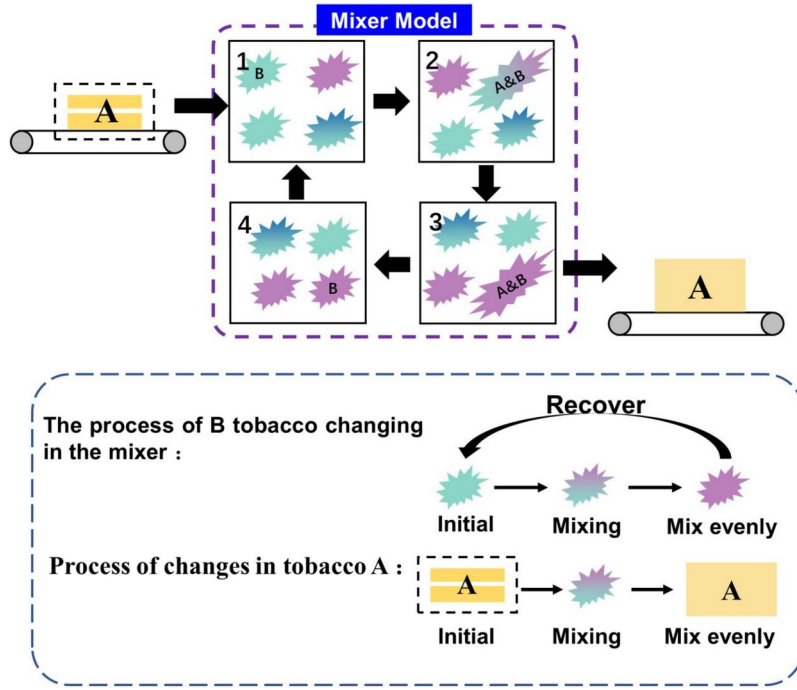


Figure 7. Schematic diagram of mixed model for winnower selection process.

tobacco at the inlet of the winnower. The tobacco (referred to as A) that entered within a unit of time mixed with B. After a certain period of time, the mixed A and B reached the same temperature and moisture content. Subsequently, A left the mixer, while B continued to move in the mixer but did not mix with the incoming tobacco until its moisture and temperature gradually returned to the mixing state.

Assuming that each piece of tobacco entering the mixer was mixed with an equal mass of B, at the end of the mixing process, A and B would have the same moisture and temperature. Based on the conservation of the total mass and energy of A and B, the following equations were obtained:

$$\left\{ \begin{array}{l} \Delta m_{t, Winnower} = m_{Winnower} + F_{t, dry}(1 + X_{Conveyor})\Delta t \\ \quad - Evap_{Winnower} - m'_{Winnower} \\ \quad - F_{t, dry}(1 + X_{cool})\Delta t \\ \Delta E_{t, Winnower} = E_{Winnower} + h_{t, Winnower, in}\Delta t \\ \quad - Q_{conv, Winnower} - Q_{evap, Winnower} \\ \quad - h_{t, Winnower, out}\Delta t - E'_{Winnower} \end{array} \right. \quad (28)$$

where  $\Delta t$  was the tobacco's time in this section,  $m_{t, Winnower}$  denoted as the inherent mass of B before mixing (Equation 29),  $m'_{Winnower}$  represented the mass of B after mixing (Equation 30), and  $Evap_{Winnower}$  was the total moisture evaporation mass (Equation 31).  $t_{Winnower}$  denoted as the residence time of the tobacco in the winnower, equal to  $\Delta t$  in this section.

$$m_{Winnower} = m_{Winnower, dry}(1 + X_{Winnower}) \quad (29)$$

$$m'_{Winnower} = m_{Winnower, dry}(1 + X_{cool}) \quad (30)$$

$$Evap_{Winnower} = R_{evap, Winnower}t_{Winnower} \quad (31)$$

$E_{Winnower}$  denoted as the heat of B before mixing (Equation 32), and  $E'_{Winnower}$  was the heat of B after mixing (Equation 33).

$$E_{Winnower} = C_p(X_{Winnower})m_{Winnower}(1 + X_{Winnower})T_{Winnower} \quad (32)$$

$$E'_{Winnower} = C_p(X_{cool})m'_{Winnower}(1 + X_{cool})T_{cool} \quad (33)$$

The formulas for A's enthalpy were listed in Equations 34 and 35.

$$h_{t, Winnower, in} = C_p(X_{Conveyor})m_{Conveyor}(1 + X_{Conveyor})T_{Conveyor} \quad (34)$$

$$h_{t, Winnower, out} = C_p(X_{cool})m_{cool}(1 + X_{cool})T_{cool} \quad (35)$$

Since the inside of the winnower was a negative pressure environment, a large amount of ambient air will enter the winnower from the inlet and outlet, so it was assumed here that the temperature inside the winnower ( $T_{Winnower}$ ) and  $T_{air}$  were equal. Since the tobacco in the winnower was thoroughly blown out and the surface area cannot be estimated, in this paper, the area and heat transfer coefficient were synthesized into a model parameter  $h_{Winnower}$ . The formula was shown below:

$$Q_{conv, Winnower} = h_{Winnower}(T_{Winnower} - T_{air})\Delta t \quad (36)$$

For the currently unknown evaporation rate formula  $R_{evap, Winnower}$ , an equation was fitted for the difference in temperature between the tobacco and winnower, tobacco moisture and equilibrium moisture correlation as shown in Equation 37:

$$R_{evap, Winnower} = \theta_{R1} \exp(\theta_{R2}(T_{Winnower, mid} - T_{air})) (X_{Winnower, mid} - X_e)^{\theta_{R3}} \quad (37)$$

where  $\theta_{R1}$ ,  $\theta_{R2}$  and  $\theta_{R3}$  were model parameters. The formulate for the median moisture  $X_{Winnower, mid}$  and the median temperature  $T_{Winnower, mid}$  in the winnower process were shown in Equation 38 and Equation 39, and  $\lambda_9$ ,  $\lambda_{10}$ ,  $\lambda_{11}$  and  $\lambda_{12}$  were used as the model parameters for the estimation of the median values.

$$X_{Winnower, mid} = \frac{\lambda_9(kX_{HDT} + (1-k)X_{Conveyor}) + \lambda_{10}X_{cool}}{\lambda_9 + \lambda_{10}} \quad (38)$$

$$T_{Winnower, mid} = \frac{\lambda_{11} \left( \frac{(1+X_{Conveyor})T_{Conveyor} + (1+X_{HDT})T_{HDT}}{1+X_{Winnower, in}} \right) + \lambda_{12}T_{cool}}{\lambda_{11} + \lambda_{12}} \quad (39)$$

### 3.2. Model parameters fitting

#### 3.2.1. Parameter optimization problem definition

State equations for the tobacco in the HDT dryer section (Equation 1), the outfeed conveyor section (Equations 20, 23) and the winnower process (Equation 28) were represented as  $f_{HDT}$ ,  $f_{Conveyor}$ , and  $f_{Winnower}$ , respectively. In the steady-state process, the incremental mass and energy of the tobacco were considered zero. To efficiently fit the model's parameters, the targeting method was used to solve these equations, with mass and energy conservation as constraints. The equations, estimated model states, and parameters were treated as decision variables, and a nonlinear least squares method was applied to minimize model errors.

The state equations consisting of 3 sets of equations of state were denoted as  $\mathcal{F}$ ,  $\mathcal{F} = [f_{HDT}, f_{Conveyor}, f_{Winnower}]$ .

The model's input variables, denoted as  $\mathcal{X}$ , included  $F_{t, inlet}$ ,  $X_{inlet}$ ,  $T_{inlet}$  and  $T_{hot}$ , thereby  $\mathcal{X} = [F_{t, inlet}, X_{inlet}, T_{inlet}, T_{hot}]$ .

There were 6 six estimated states of the steady-state model, which were denoted as  $\hat{y}$ ,  $\hat{y} = [\hat{X}_{HDT}, \hat{T}_{HDT}, \hat{X}_{Conveyor}, \hat{T}_{Conveyor}, \hat{X}_{cool}, \hat{T}_{cool}]$ . And the actual state was denoted as  $y$ ,  $y = [X_{HDT}, T_{HDT}, X_{Conveyor}, T_{Conveyor}, X_{cool}, T_{cool}]$ .

The whole model contained a total of 44 parameters to be fitted, denoted as  $\Theta$ . The decision variable was denoted as  $p$ , where  $p = [\Theta, \hat{y}]$ .

In summary, the mechanistic model can be expressed as  $\hat{y} = \mathcal{F}(\mathcal{X}, p)$ .

In order to find the optimal model parameters, the residuals between the model predictions and the actual measurements were minimized. The objective function for the optimization problem was:

$$\mathcal{J} = (y - \hat{y})^2 = (y - F(\mathcal{X}, p))^2 \quad (40)$$

In Matlab, the interior point method in `fmincon` was used as an optimization algorithm to continuously optimize the decision variables by minimizing  $\mathcal{J}$ :

$$\hat{p}_{opt} = \underset{p}{\operatorname{argmin}} \mathcal{J} = \underset{p}{\operatorname{argmin}} (y - F(\mathcal{X}, p))^2 \quad (41)$$

For the nonlinear constraints in the optimization problem and the bounds on model parameters, some were derived from research studies. Among the 44 parameters, six were associated with the density calculation formula, four were linked to the water activity of tobacco, three pertained to equilibrium moisture, five were related to the water diffusion coefficient, and two concerned the specific heat of tobacco. Due to the inability to experimentally determine the intrinsic relationships among moisture, temperature, density, water activity, equilibrium moisture, specific heat capacity, and moisture diffusion coefficient in tobacco, functional correlation equations proposed by other scholars were cited. The physical and chemical properties of the tobacco under study differed from those of other materials being investigated, and the parameter values also varied accordingly. However, to ensure the rationality of the parameters, the optimization range of these 20 parameters was maintained within the same order of magnitude as the drying property parameters of other materials. Additionally, constraints on density, water activity, equilibrium moisture, and water diffusion coefficient were imposed to ensure practical physical meaning. For instance, the water activity of tobacco was constrained to a range of 0 to 1. Detailed constraints were shown below:

$$\begin{cases} 200 < \rho_t(X_{HDT}, T_{HDT}, \Theta) < 800 \\ 0 < a_w(X_{HDT}, T_{HDT}, \Theta) < 1 \\ D_{eff}(T_{HDT}, \Theta) > 0 \\ D_{eff}(T_{Conveyor}, \Theta) > 0 \\ X_e(T_{HDT}, \Theta) > 0 \\ X_e(T_{Winnower}, \Theta) > 0 \end{cases} \quad (42)$$



### 3.2.2. Fitting results

Available data from 25 production batches of a particular tobacco brand required fitting 44 model parameters. The dataset comprised a total of 75 samples, including 3 samples that contained complete key process variables. 60 samples were selected for training, and rest samples were used for testing.

The nonlinear least squares method was applied to fit the model parameters, with the fitting parameters were list in Table 2 and the fitting results detailed in Table 3. As for the parameters of winnower section, for the parameters of the winnower, the physical process was to mix and average the tobacco entering the winnower with the tobacco inside, which had a mass of 0.050 kg, a moisture content of 0.1365, and a temperature of 301 K. Moreover, there were no abnormalities in the model parameters such as the heat transfer coefficient, mass transfer coefficient, and the characteristic length of the tobacco. According to the fitting results in Table 3, the prediction error of  $X_{cool}$  was the smallest, generally within  $5.000 \times 10^{-4}$ , indicating that the model also accurately predicted  $X_{HDT}$  and  $T_{HDT}$ . Although there were insufficient measurement samples for  $X_{Conveyor}$ ,  $T_{Conveyor}$  and  $T_{cool}$ , the estimated values for these states were very close to the true values and deemed reasonable.

## 4. Monte Carlo simulation based model validation

### 4.1. Kernel density estimation

During HDT pneumatic drying process, the relative positions of tobacco leaves often shifted, meaning moisture meters at different locations might not measure the same portion of tobacco. In addition, due to the small measurement area of the infrared moisture meter and the uneven distribution of moisture and temperature in the tobacco, the timing data obtained from the moisture meter lacked representativeness, as illustrated in Figure 8. In order to accurately assess tobacco's moisture content, it was necessary to analyze the statistical distribution characteristics of the moisture data throughout the entire tobacco process.

Firstly, given the assumption that the difference in the distribution of moisture in the radial and axial directions was not caused by mechanistic factors, and the distribution of the entire batch was approximated to the statistical distribution of the measured samples. Then, kernel density estimation, a non-parametric statistical technique, was used to estimate the probability density function of a random variable based on given sample of data points, without making any

assumptions about the distribution form. Its formula was given below:

$$\hat{f}(x) = \frac{1}{nh} \sum_{i=1}^n K\left(\frac{x-x_i}{h}\right) \quad (43)$$

In this equation,  $x$  represented the location where the density was to be estimated,  $x_i$  denoted as a sample data point,  $\hat{f}(x)$  was the estimated density at point  $x$ ,  $n$  was the number of sample data points,  $h$  was the bandwidth parameter, and  $K(\cdot)$  was the kernel function. Since the probability density of tobacco moisture content data might not have conformed to a specific distribution, KDE method was advantageous as it did not require any pre-assumptions about the form of the distribution. Instead, it estimated the probability density function solely based on the data, constructing a smooth and accurate density function curve by calculating the contribution of each sample point to the overall density, as shown in Equation 44.

$$K(x) = \frac{1}{\sqrt{2\pi}} \exp\left(-\frac{x^2}{2}\right) \quad (44)$$

To minimize the mean square error between the estimated and actual probability density functions, the bandwidth  $h$  was selected using the Rule of Thumb (ROT) method. For univariate data, a Gaussian kernel function was employed, and the optimal bandwidth  $h_{opt}$  was determined in Equation 45, and  $\hat{\sigma}$  represented the standard deviation of the data sample, IQR denoted the interquartile range. And in this work, IQR was  $1.400 \times 10^{-3}$ .

$$h_{opt} = 0.9 \min\left(\hat{\sigma}, \frac{IQR}{1.34}\right) n^{-\frac{1}{5}} \quad (45)$$

With KDE method, it was available to get the probability density function of the tobacco's moisture content and then generate random samples.

### 4.2. Monte Carlo method

Monte Carlo simulation was a numerical technique used to model system behavior through random sampling. By generating numerous random samples within a specified parameter range, it evaluated the system's performance and output.<sup>[22]</sup> In the previous section,  $X_{inlet}$  and  $L_t$  were identified as key factors influencing moisture fluctuations after drying. To assess the predictive accuracy of the steady-state drying model, random samples of  $X_{inlet}$ , based on its probability distribution, and  $L_t$  were generated to simulate real production conditions. These simulated

**Table 3.** Model fitting results.

Batch	Usage	$X_{HDT}$		$T_{HDT}$ (K)		$X_{Conveyor}$		$T_{Conveyor}$ (K)		$X_{cool}$ (K)		$T_{cool}$ (K)	
		Actual	Predict	Actual	Predict	Actual	Predict	Actual	Predict	Actual	Predict	Actual	Predict
1	training	1.448	1.449	3.384	3.382	1.194	1.194	3.256	3.257	1.377	1.377	3.073	3.076
2	training	1.451	1.450	3.387	3.382	1.194	1.194	3.257	3.258	1.377	1.377	3.074	3.076
3	test	1.448	1.449	3.386	3.381	1.192	1.194	3.260	3.257	1.376	1.377	3.074	3.076
4	training	1.441	1.443	3.385	1.377	-	1.197	-	3.251	1.375	1.376	-	3.073
5	training	1.449	1.444	3.386	3.377	-	1.197	-	3.252	1.377	1.376	-	3.073
6	training	1.446	1.444	3.388	3.378	-	1.197	-	3.252	1.375	1.376	-	3.073
7	training	1.427	1.447	3.375	3.380	-	1.195	-	3.255	1.375	1.377	-	3.074
8	training	1.433	1.447	3.379	3.379	-	1.196	-	3.254	1.372	1.377	-	3.074
9	test	1.451	1.446	3.383	3.379	-	1.196	-	3.254	1.381	1.377	-	3.074
10	test	1.445	1.438	3.384	3.375	-	1.199	-	3.249	1.372	1.375	-	3.071
11	training	1.440	1.439	3.384	3.376	-	1.198	-	3.250	1.383	1.376	-	3.072
12	training	1.422	1.431	3.378	3.373	-	1.200	-	3.246	1.374	1.374	-	3.070
13	training	1.445	1.446	3.383	3.383	-	1.196	-	3.254	1.376	1.377	-	3.074
14	training	1.443	1.447	3.385	3.380	-	1.195	-	3.255	1.377	3.074	-	3.074
15	training	1.432	1.446	3.376	3.379	-	1.196	-	3.254	1.376	1.377	-	3.074
16	training	1.438	1.442	3.380	3.377	-	1.197	-	3.251	1.376	1.376	-	3.073
17	training	1.442	1.441	3.380	3.376	-	1.198	-	3.251	1.377	1.376	-	3.072
18	training	1.442	1.449	3.385	3.383	-	1.195	-	3.256	1.377	1.377	-	3.075
19	training	1.448	1.443	3.383	3.378	-	1.196	-	3.253	1.377	1.376	-	3.073
20	training	1.449	1.450	3.383	3.382	-	1.194	-	3.258	1.376	1.377	-	3.075
21	training	1.445	1.447	3.385	3.380	-	1.195	-	3.254	1.376	1.377	-	3.074
22	training	1.448	1.449	3.385	3.382	-	1.194	-	3.256	1.377	1.377	-	3.074
23	training	1.450	1.446	3.386	3.379	-	1.196	-	3.253	1.377	1.377	-	3.074
24	test	1.444	1.446	3.386	3.379	-	1.196	-	3.254	1.376	1.377	-	3.074
25	test	1.450	1.448	3.385	3.380	-	1.195	-	3.255	1.378	1.377	-	3.075
26	test	1.445	1.447	3.386	3.380	-	1.195	-	3.254	1.376	1.377	-	3.074
27	training	1.445	1.448	3.386	3.381	-	1.195	-	3.256	1.377	1.377	-	3.075
28	training	1.448	1.444	3.385	3.378	-	1.197	-	3.252	1.377	1.376	-	3.073
29	training	1.446	1.444	3.385	3.378	-	1.197	-	3.252	1.377	1.376	-	3.073
30	training	1.451	1.441	3.385	3.376	-	1.198	-	3.250	1.376	1.376	-	3.072
31	training	1.441	1.449	3.375	3.382	-	1.194	-	3.257	1.376	1.377	-	3.076
32	training	1.442	1.449	3.374	3.382	-	1.194	-	3.256	1.377	1.377	-	3.075
33	training	1.439	1.448	3.373	3.381	-	1.195	-	3.255	1.377	1.377	-	3.075
34	training	1.463	1.453	3.394	3.387	-	1.191	-	3.261	1.376	1.377	-	3.078
35	training	1.458	1.452	3.393	3.387	-	1.191	-	3.261	1.376	1.377	-	3.078
36	training	1.459	1.452	3.394	3.386	-	1.191	-	3.260	1.376	1.377	-	3.077
37	training	1.457	1.452	3.386	3.387	-	1.191	-	3.261	1.379	1.377	-	3.078
38	training	1.452	1.453	3.386	3.389	-	1.190	-	3.262	1.376	1.376	-	3.078
39	training	1.455	1.453	3.385	3.389	-	1.190	-	3.262	1.377	1.376	-	3.078
40	training	1.450	1.452	3.385	3.387	-	1.191	-	3.261	1.376	1.376	-	3.078
41	training	1.456	1.452	3.384	3.387	-	1.191	-	3.261	1.377	1.376	-	3.078
42	training	1.457	1.452	3.383	3.386	-	1.192	-	3.260	1.377	1.377	-	3.077
43	test	1.460	1.453	3.392	3.390	-	1.189	-	3.263	1.377	1.376	-	3.079
44	training	1.461	1.453	3.392	3.387	-	1.190	-	3.261	1.175	1.376	-	3.078
45	training	1.461	1.453	3.389	3.388	-	1.190	-	3.261	1.377	1.376	-	3.078
46	training	1.463	1.450	3.387	3.384	-	1.193	-	3.258	1.377	1.377	-	3.076
47	training	1.461	1.451	3.386	3.384	-	1.192	-	3.259	1.376	1.377	-	3.077
48	training	1.463	1.450	3.384	3.384	-	1.193	-	3.258	1.377	1.377	-	3.076
49	training	1.442	1.450	3.374	3.383	-	1.193	-	3.257	1.377	1.377	-	3.076
50	training	1.442	1.449	3.377	3.381	-	1.194	-	3.256	1.377	1.377	-	3.075
51	training	1.437	1.449	3.372	3.381	-	1.194	-	3.256	1.375	1.377	-	3.075
52	training	1.432	1.453	3.373	3.392	-	1.188	-	3.264	1.377	1.376	-	3.080
53	training	1.445	1.453	3.378	3.398	-	1.187	-	3.265	1.377	1.375	-	3.080
54	test	1.441	1.453	3.375	3.392	-	1.188	-	3.264	1.376	1.376	-	3.080
55	test	1.459	1.451	3.378	3.385	-	1.192	-	3.259	1.378	1.377	-	3.077
56	test	1.459	1.451	3.379	3.384	-	1.193	-	3.258	1.376	1.377	-	3.076
57	training	1.458	1.449	3.379	3.382	-	1.194	-	3.257	1.378	1.377	-	3.075
58	training	1.454	1.452	3.378	3.385	-	1.192	-	3.260	1.377	1.377	-	3.077
59	training	1.449	1.452	3.378	3.387	-	1.191	-	3.261	1.377	1.377	-	3.078
60	training	1.454	1.452	3.383	3.386	-	1.191	-	3.260	1.376	1.377	-	3.077
61	training	1.456	1.453	3.382	3.389	-	1.189	-	3.263	1.378	1.376	-	3.079
62	training	1.457	1.453	3.384	3.389	-	1.190	-	3.262	1.376	1.376	-	3.079
63	training	1.454	1.453	3.384	3.390	-	1.189	-	3.263	1.376	1.377	-	3.079
64	training	1.450	1.454	3.388	3.390	-	1.189	-	3.263	1.377	1.377	-	3.079
65	training	1.456	1.454	3.387	3.390	-	1.189	-	3.263	1.377	1.377	-	3.079
66	training	1.450	1.453	3.384	3.390	-	1.189	-	3.263	1.376	1.377	-	3.079
67	training	1.450	1.452	3.387	3.386	-	1.191	-	3.260	1.376	1.377	-	3.077
68	training	1.451	1.453	3.385	3.387	-	1.191	-	3.261	1.376	1.377	-	3.078
69	training	1.452	1.453	3.386	3.387	-	1.191	-	3.261	1.379	1.377	-	3.078
70	training	1.448	1.443	3.378	3.377	-	1.197	-	3.252	1.376	1.376	-	3.073
71	training	1.445	1.443	3.377	3.377	-	1.197	-	3.252	1.377	1.376	-	3.073
72	training	1.451	1.443	3.379	3.377	-	1.197	-	3.252	1.376	1.376	-	3.073
73	training	1.448	1.451	3.377	3.385	-	1.192	-	3.259	1.377	1.376	-	3.077
74	training	1.451	1.451	3.377	3.385	-	1.192	-	3.259	1.377	1.377	-	3.077
75	training	1.448	1.450	3.373	3.383	-	1.193	-	3.257	1.377	1.376	-	3.076

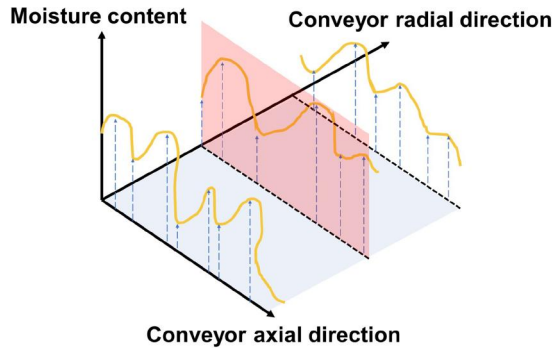


**Figure 8.** Schematic diagram of moisture content distribution in tobacco on the conveyor (red area represented the moisture content within the sampling area).

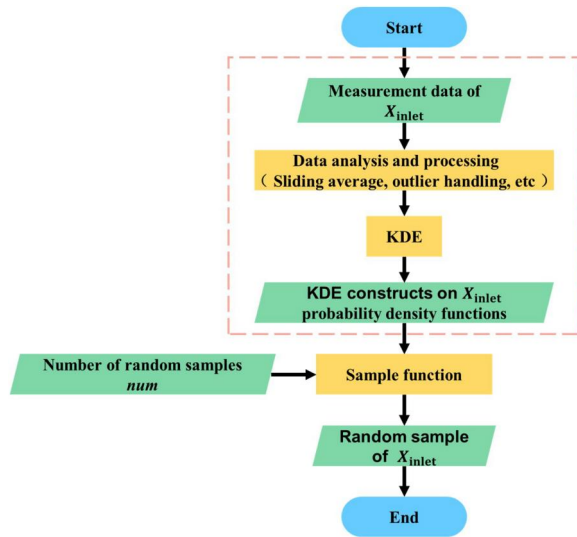


**Figure 9.** Random sampling of tobacco's moisture at the inlet of the dryer.

results were then compared with actual tobacco moisture data to evaluate the model's validity.

In the simulation,  $F_{inlet}$  remained constant as a fixed input,  $X_{inlet}$  was treated as a stochastic variable due to measurement limitations and inherent moisture distribution variability. And  $L_t$  was also a stochastic variable owing to the phenomena observed during the experimental process.

The steps for generating random samples of  $X_{inlet}$  using Monte Carlo simulation were outlined in Figure 9.

Firstly, time series data for  $X_{inlet}$  was collected from the inlet moisture meter. Secondly, data processing methods, such as applying a sliding average to reduce measurement noise, were then employed. Thirdly, random samples of  $X_{inlet}$  were generated using the KDE toolbox in Matlab, which processed the timing data to produce a KDE structure representing the probability density of  $X_{inlet}$ . The Matlab sample

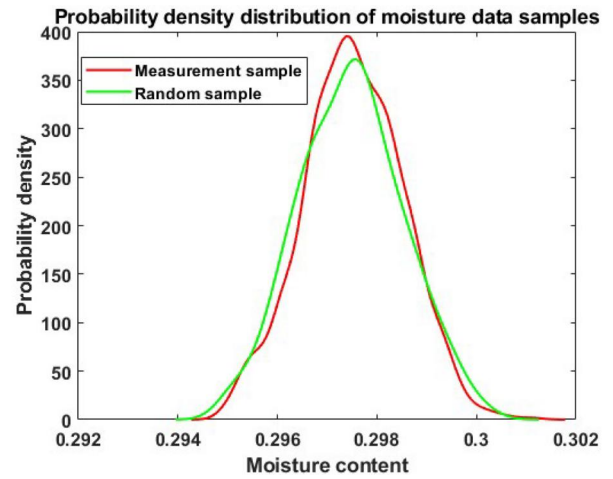


**Figure 10.** Probability density distribution of moisture measurement samples and random samples at the entrance of the dryer.

function was used to generate the desired number of random samples based on this KDE structure.

Here, using data from a specific test batch, 500 Monte Carlo random samples were generated based on real data samples of  $X_{inlet}$ . The actual probability distribution and the probability density distribution of the random samples were shown in Figure 10. The mean of the  $X_{inlet}$  random samples was  $2.975 \times 10^{-1}$ , with a variance of  $1.089 \times 10^{-6}$ , which closely matched the distribution of the real samples.

$L_t$  was a model parameter defining the shape of tobacco particles, differed from the actual tobacco length, and could not be directly measured. In steady-state modeling,  $L_t$  was assumed to be constant throughout the process and was determined through nonlinear least squares fitting. Since  $L_t$  was a stochastic variable in the simulation, it was reasonable to assume that  $L_t$  followed a normal distribution with a mean of  $4.079 \times 10^{-2}$  and a variance of  $5.500 \times 10^{-3}$ .

### 4.3. Monte Carlo simulation based model testing

Using the data from the batch with complete key process variables, 500 samples were generated through Monte Carlo random sampling and input into the steady-state model for calculation. The statistical results were presented in Table 4 and Figure 11.

The Monte Carlo simulation results indicated that the steady-state model could relatively accurately estimate the mean values of the state distribution of tobacco at various points: the outlet of the dryer, and the inlet and outlet of the winnower. Notably for  $X_{cool}$ , the mean error in predicting the cooling moisture was  $1.000 \times 10^{-4}$ .

Additionally, Monte Carlo simulation was also performed on select data samples from the test set to verify the effectiveness of the steady-state model. For example, the statistical results for other three batches (the 8th, 11th, and 17th batches) of the drying process were shown in Table 5. The results from the Monte Carlo simulation indicated that the model was able to accurately estimate the cooling moisture of the tobacco. The estimation errors for  $X_{HDT}$  and  $T_{HDT}$  were minimal, and mean values of  $\hat{X}_{Conveyor}$  and  $\hat{T}_{Conveyor}$  were reasonable (Figure 12).

**Table 4.** Monte Carlo simulation results of the first batch of pneumatic drying process.

State of tobacco	Actual mean value	Predicted mean value
Outlet moisture of the dryer ( $10^{-1}$ )	1.449	1.452
Outlet temperature of the dryer ( $10^2$ K)	3.386	3.381
Inlet moisture of the winnower ( $10^{-1}$ )	1.193	1.194
Inlet temperature of the dryer ( $10^2$ K)	3.257	3.257
Cooling moisture ( $10^{-1}$ )	1.377	1.378
Cooling temperature ( $10^2$ K)	3.073	3.075

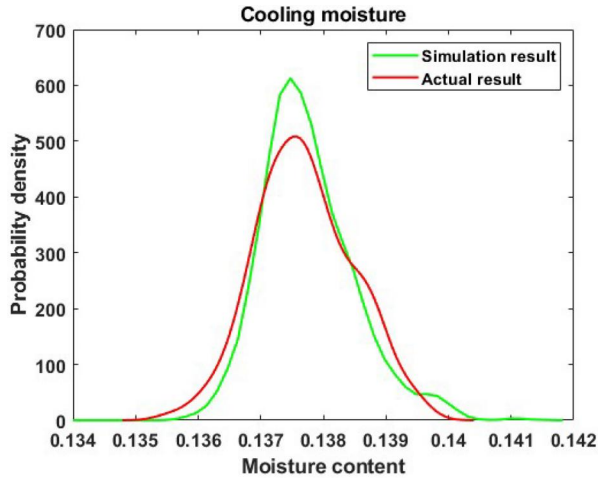


**Figure 11.** Monte Carlo Simulation for the First Batch.

## 5. Model-based feedforward control for HDT pneumatic drying process

### 5.1. Model-based feedforward control strategy

The original control strategy at the cigarette factory did not adequately account for the effects of fluctuations in tobacco feed on the drying process. As a result, the control of cooling moisture was ineffective and did not meet the upgraded product quality requirements. To address this issue, a feed-forward control was integrated into the existing control system based on the steady-state model in Equation 46 (mainly combined with Equations 1, 20, 23 and 28) and  $X$  represented the process variables that needed to be input into the model to predict cooling moisture, which was consist of  $F_{t,inlet}$ ,  $X_{inlet}$  and  $T_{hot}$ .

$$\begin{aligned} \hat{X}_{cool} &= \mathcal{F}(X, \Theta) \\ X &= [F_{t,inlet}, X_{inlet}, T_{hot}] \end{aligned} \quad (46)$$

This enhancement aimed to reduce the impact of variations in tobacco input on the drying process in the HDT dryer. The improved control structure was illustrated in Figure 13.

The feedforward coefficients were determined by performing linear regression on a large history dataset. This dataset included the 100-fold difference between  $\bar{X}_{inlet}$  (the mean value of  $X_{inlet}$ ) and  $\bar{X}_{cool}$  (the mean value of  $X_{cool}$ ). To account for the percentage-based representation of moisture content, the values were multiplied by 100 before being correlated with  $\bar{u}_{feedforward}$ . The regression equation was given by:

$$\bar{u}_{feedforward} = K(\bar{X}_{inlet} - \bar{X}_{cool}) \times 100 + b \quad (47)$$

According to the history data, the regression analysis yielded a coefficient  $K=2.337$  and an intercept  $b=2.550$ .  $\Theta$  was also fitted by historical data, with

**Table 5.** Monte Carlo simulation results for other three batches.

Data batch	Tobacco state	Actual mean	Predicted mean
8	Outlet moisture of the dryer ( $10^{-1}$ )	$1.450 \times 10^{-1}$	$1.439 \times 10^{-1}$
	Outlet temperature of the dryer ( $10^2$ K)	$3.386 \times 10^2$	$3.378 \times 10^2$
	Inlet moisture of the winnower ( $10^{-1}$ )	-	$1.196 \times 10^{-1}$
	Inlet temperature of the dryer ( $10^2$ K)	-	$3.252 \times 10^2$
	Cooling moisture ( $10^{-1}$ )	$1.377 \times 10^{-1}$	$1.375 \times 10^{-1}$
	Cooling temperature ( $10^2$ K)	$3.073 \times 10^2$	$3.073 \times 10^2$
11	Outlet moisture of the dryer ( $10^{-1}$ )	$1.450 \times 10^{-1}$	$1.445 \times 10^{-1}$
	Outlet temperature of the dryer ( $10^2$ K)	$3.386 \times 10^2$	$3.382 \times 10^2$
	Inlet moisture of the winnower ( $10^{-1}$ )	-	$1.194 \times 10^{-1}$
	Inlet temperature of the dryer ( $10^2$ K)	-	$3.256 \times 10^2$
	Cooling moisture ( $10^{-1}$ )	$1.377 \times 10^{-1}$	$1.375 \times 10^{-1}$
	Cooling temperature ( $10^2$ K)	-	$3.075 \times 10^2$
17	Outlet moisture of the dryer ( $10^{-1}$ )	$1.450 \times 10^{-1}$	$1.447 \times 10^{-1}$
	Outlet temperature of the dryer ( $10^2$ K)	$3.386 \times 10^2$	$3.381 \times 10^2$
	Inlet moisture of the winnower ( $10^{-1}$ )	-	$1.194 \times 10^{-1}$
	Inlet temperature of the dryer ( $10^2$ K)	-	$3.256 \times 10^2$
	Cooling moisture ( $10^{-1}$ )	$1.377 \times 10^{-1}$	$1.376 \times 10^{-1}$
	Cooling temperature ( $10^2$ K)	-	$3.075 \times 10^2$



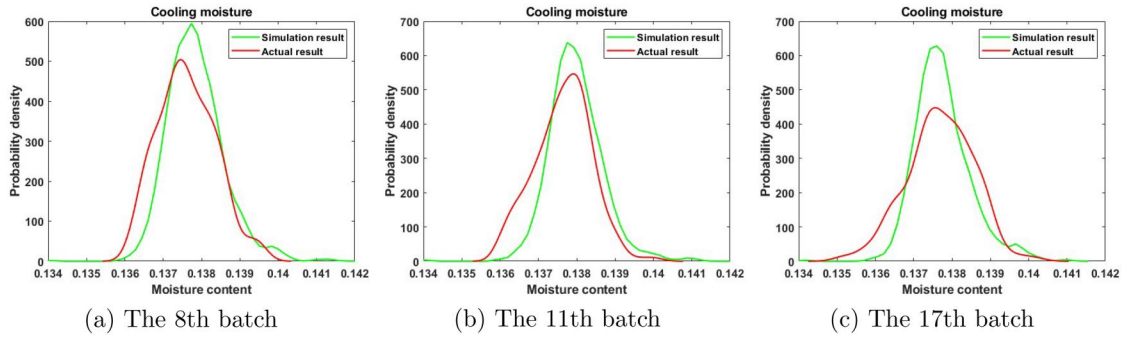


Figure 12. Monte Carlo Simulation for other three batches.

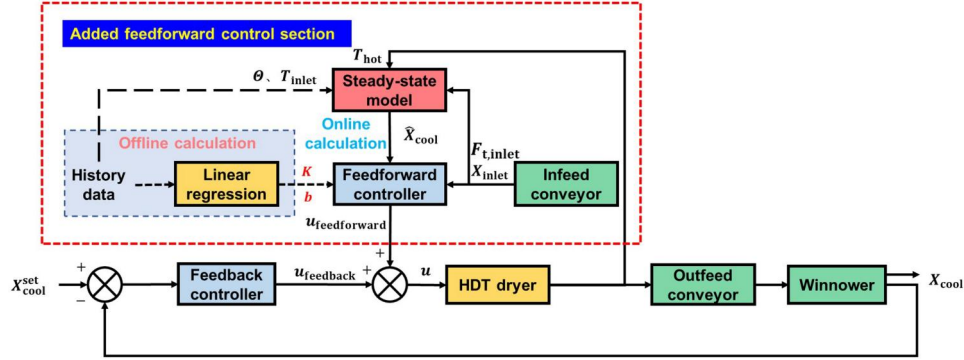


Figure 13. Improved control system structure.

$T_{inlet}$  being fixed as a constant value.  $\hat{X}_{cool}$  can be computed online based on the steady-state model and measurement values, such as  $F_{t,in}$ ,  $X_{inlet}$  and  $T_{hot}$ .  $u_{feedforward}$  was calculated based on  $\hat{X}_{cool}$ ,  $T_{hot}$  and coefficients  $K$  and  $b$ , as shown in Equation 48.

$$u_{feedforward} = K(X_{inlet} - \hat{X}_{cool}) \times 100 + b \quad (48)$$

Simultaneously, the feedback controller adjusted  $u_{feedback}$  based on the deviation between  $X_{cool}^{set}$  and  $X_{cool}$ .  $u_{feedforward}$  was combined with  $u_{feedback}$  to obtain the total control input,  $u$ , which was then applied to the HDT dryer. This enhanced control system enabled timely adjustments to  $u$  based on  $X_{inlet}$ , thereby significantly improving control efficiency.

## 5.2. Moisture content control results of improved control system

The  $X_{cool}$  standard deviation probability density distribution plotted based on KDE method for 214 batches of  $X_{cool}$  data before the control structure improvement and all batches of  $X_{cool}$  data after the improvement were counted. Under the original control scheme (shown by the blue line on the way), the mean value of the  $X_{cool}$  standard deviation was  $6.220 \times 10^{-4}$ , and the standard deviation was  $8.626 \times 10^{-5}$ , with an overall right-skewed distribution and a long right trailing tail, which indicated that the consistency of

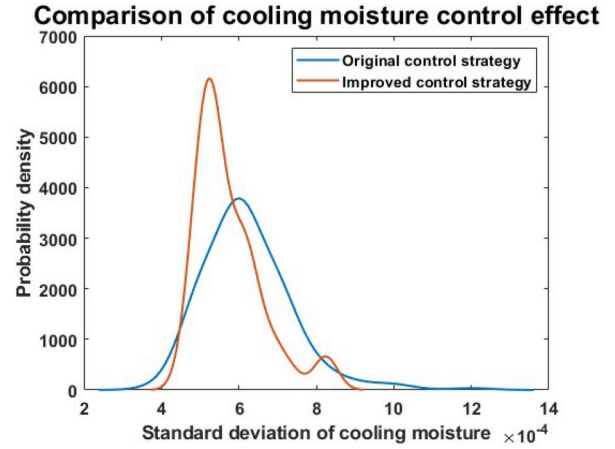


Figure 14. Comparison of cooling water control effects.

$X_{cool}$  within different batches was poorer. The ability of the original control scheme to regulate  $X_{cool}$  fluctuations was limited, and it was unable to effectively reduce moisture fluctuations when fluctuations in the tobacco feed occurred (Figure 14).

After the improvement of the control strategy, the standard deviation of  $X_{cool}$  was  $5.744 \times 10^{-4}$ , and the standard deviation was  $8.626 \times 10^{-5}$ . Comparing the distribution of the standard deviation of  $X_{cool}$  before and after the improvement of the control strategy, the mean value of the standard deviation reduced by 7.65%, the standard deviation reduced by 20.27%, and

the differences in the standard deviation of  $X_{cool}$  in different batches significantly reduced.

It can be seen that the feedforward control based on the steady state model can effectively reduce the standard deviation of  $X_{cool}$  within a batch by compensating for the random disturbance in the HDT dryer in time, and also greatly improve the consistency of  $X_{cool}$  within different batches.

## 6. Conclusion

The paper introduced a steady-state process model for the HDT dryer focused on moisture control in tobacco drying. The main innovation was creating a first-principles-based steady-state model and applying it to real-world tobacco drying processes, effectively enhancing the control of cooling moisture fluctuations and assessing the model's performance in practical scenarios.

The study began by describing the HDT dryer and detailing the drying process, which was divided into three sections. With a FLIR thermal camera, the temperature field at the infrared moisture meter's measurement point was observed, revealing a non-uniform temperature distribution and poor data representativeness. Under such condition, a steady-state model was developed based on mass and energy conservation principles to calculate the moisture and temperature of tobacco. In this model, tobacco was represented as cylindrical particles within the dryer, with stable gas properties assumed throughout the process. Analysis revealed that the inlet moisture and the tobacco's characteristic length significantly affected post-drying moisture fluctuations. In the outfeed conveyor section, a moisture meter was temporarily installed at the winnower inlet to verify the layered model, which focused heat and mass transfer in the upper layer, with moisture loss computed using Fick's second law. A specialized mixer model was employed for the winnower to minimize state fluctuations. The model's parameters were obtained through nonlinear least squares methods. The steady-state model accurately estimated cooling moisture and effectively predicted other states throughout the drying process.

For controlling cooling moisture fluctuations, the steady-state model was used to estimate cooling moisture online, with a feedforward controller adjusting outputs based on this estimate. Post-control scheme improvement, the mean standard deviation of cooling moisture decreased by 7.65%, and the overall standard deviation reduced by 20.27%. This feedforward control effectively minimized cooling moisture variability

within batches and enhanced consistency across different batches of tobacco.

## Nomenclature

### Symbols

$a_w$	Activity of moisture
$A$	Area ( $m^2$ )
$B$	Parameter of diffusion coefficient calculation model ( $m^2s^{-1}$ )
$C_p$	Heat capacity of tobacco ( $kJ/kg$ )
$D_{eff}$	Effective diffusion coefficient ( $m^2s^{-1}$ )
$E$	Energy ( $kJ$ )
$E_a$	Activation energy ( $kJ$ )
$F$	Mass flow ( $kg/s$ )
$H$	Humidity (kg water / kg dried gas)
$h$	Heat transfer coefficient ( $kJ/(Km^2)$ )
$h_t$	Enthalpy flow of tobacco ( $kJ/s$ )
$k$	Ratio of dry weight of upper and lower cut tobacco
$k_{HDT}$	Mass transfer coefficient in HDT section ( $kg/s$ )
$L$	Latent heat ( $kJ$ )
$L_t$	Characteristic length ( $m$ )
$L^{thick}$	Thickness of tobacco ( $m$ )
$MR$	Moisture ratio
$m$	Mass ( $kg$ )
$P$	Pressure ( $Pa$ )
$Q$	Quality of heat ( $kJ$ )
$r$	The radius of cylindrical particles ( $m$ )
$R$	Ideal gas constant ( $J/(molK)$ )
$RH$	Relative humidity
$t$	Time ( $s$ )
$T$	Temperature ( $K$ )
$u$	Control variable
$V$	Volume ( $m^3$ )
$W$	Evaporation rate ( $kg/s$ )
$X$	Moisture content of tobacco
$X_e$	Equilibrium moisture
$X_0$	Initial moisture

### Greek Symbols

$\rho$	Density ( $kg/m^3$ )
$\theta$	Parameter

### Subscripts

<i>cool</i>	Cooling state at the outlet of the winnower
<i>Conveyor</i>	Outfeed conveyor section
<i>dry</i>	Dry basis of the matter
<i>evap</i>	Evaporation
<i>g</i>	Gas
<i>HDT</i>	The HDT dryer section.
<i>hot</i>	Hot wind
<i>inlet</i>	The inlet of the HDT dryer
<i>l</i>	Liquid
<i>sat</i>	Saturated
<i>set</i>	Set value
<i>t</i>	Tobacco
<i>v</i>	Vapor
<i>Winnower</i>	Winnower section



## Disclosure statement

No potential conflict of interest was reported by the author(s).

## Funding

The authors gratefully acknowledge the financial support from the Institute of Zhejiang University-Quzhou Science and Technology Project (Nos. IZQ2022KYZX12 and IZQ2022KJ3001).

## References

- [1] Friso, D. Mathematical Modelling of Rotary Drum Dryers for Alfalfa Drying Process Control. *Inventions* **2023**, *8*, 11. DOI: [10.3390/inventions8010011](https://doi.org/10.3390/inventions8010011).
- [2] Tarasiewicz, S.; Léger, F. Modeling Simulation and Control of the Wood Drying process - Part 1. A Set of PDE's as an Internal Model. *Drying Technol.* **1998**, *16*, 1075–1084. DOI: [10.1080/07373939808917454](https://doi.org/10.1080/07373939808917454).
- [3] Stawczyk, J.; Comaposada, J.; Gou, P.; Arnau, J. Fuzzy Control System for a Meat Drying Process. *Drying Process* **2004**, *22*, 259–267. DOI: [10.1081/DRT-120028232](https://doi.org/10.1081/DRT-120028232).
- [4] Yuzgec, U.; Becerikli, Y.; Turker, M. Nonlinear Predictive Control of a Drying Process Using Genetic Algorithms. *ISA Trans.* **2006**, *45*, 589–602. DOI: [10.1016/s0019-0578\(07\)60234-1](https://doi.org/10.1016/s0019-0578(07)60234-1).
- [5] Zhang, L.; Cui, H.; Li, H.; Han, F.; Zhang, Y.; Wu, W. Parameters Online Detection and Model Predictive Control during the Grain Drying Process. *Math. Probl. Eng.* **2013**, *2013*, 924698.
- [6] Bi, S.; Zhang, B.; Mu, L.; Ding, X.; Wang, J. Optimization of Tobacco Drying Process Control Based on Reinforcement Learning. *Drying Technol.* **2020**, *38*, 1291–1299. DOI: [10.1080/07373937.2019.1633662](https://doi.org/10.1080/07373937.2019.1633662).
- [7] Wu, Y.; Wu, W.; Han, F.; et al. Intelligent Monitoring and Control of Grain Continuous Drying Process Based on Multi-Parameter Corn Accumulated Temperature Model. 2017 International Conference on Smart Grid and Electrical Automation (ICSGEA), IEEE, **2017**, 77–80.
- [8] Chen, A. G.; Ren, Z. Y.; Fan, Z. P.; Xue, F. Two-Layered Model Predictive Control Strategy of the Cut Tobacco Drying Process. *IEEE Access* **2020**, *8*, 155697–155709. DOI: [10.1109/ACCESS.2020.3018476](https://doi.org/10.1109/ACCESS.2020.3018476).
- [9] Abdoli, B.; Zare, D.; Jafari, A.; Chen, G. Evaluation of the Air-Borne Ultrasound on Fluidized Bed Drying of Shelled Corn: Effectiveness, Grain Quality, and Energy Consumption. *Drying Technol.* **2018**, *36*, 1749–1766. DOI: [10.1080/07373937.2018.1423568](https://doi.org/10.1080/07373937.2018.1423568).
- [10] Banooni, S.; Hajidavalloo, E.; Dorfeshan, M. A Comprehensive Review on Modeling of Pneumatic and Flash Drying. *Drying Technol.* **2018**, *36*, 33–51. DOI: [10.1080/07373937.2017.1298123](https://doi.org/10.1080/07373937.2017.1298123).
- [11] Levy, A.; Borde, I. Two-Fluid Model for Pneumatic Drying of Particulate Materials. *Drying Technol.* **2001**, *19*, 1773–1788. DOI: [10.1081/DRT-100107272](https://doi.org/10.1081/DRT-100107272).
- [12] Gidaspow, D. *Multiphase Flow and Fluidization: Continuum and Kinetic Theory Descriptions*; New York: Academic press, **1994**.
- [13] do Carmo Ferreira, M.; Freire, J. T.; Massarani, G. Homogeneous Hydraulic and Pneumatic Conveying of Solid Particles. *Powder Technol.* **2000**, *108*, 46–54. DOI: [10.1016/S0032-5910\(99\)00245-4](https://doi.org/10.1016/S0032-5910(99)00245-4).
- [14] Levy, A.; Borde, I. Pneumatic and Flash Drying. In *Handbook of Industrial Drying*, 4th ed.; Mujumdar, A.S., Ed.; Boca Raton, FL: CRC Press, **2014**; pp 381–392.
- [15] de Pádua, T. F.; Béttega, R.; Freire, J. T. Gas-Solid Flow Behavior in a Pneumatic Conveying System for Drying Applications: Coarse Particles Feeding with a Venturi Device. *ACES.* **2015**, *05*, 225–238. DOI: [10.4236/aces.2015.53024](https://doi.org/10.4236/aces.2015.53024).
- [16] Levy, A.; Borde, I. Steady State One-Dimensional Flow Model for a Pneumatic Dryer. *Chem. Eng. Process.* **1999**, *38*, 121–130. DOI: [10.1016/S0255-2701\(98\)00079-8](https://doi.org/10.1016/S0255-2701(98)00079-8).
- [17] Martynenko, A.; Misra, N. N. Machine Learning in Drying. *Drying Technol.* **2020**, *38*, 596–609. DOI: [10.1080/07373937.2019.1690502](https://doi.org/10.1080/07373937.2019.1690502).
- [18] Tanaka, F.; Maeda, Y.; Uchino, T.; Hamanaka, D.; Atungulu, G. G. Monte Carlo Simulation of the Collective Behavior of Food Particles in Pneumatic Drying Operation. *LWT-Food Sci. Technol.* **2008**, *41*, 1567–1574. DOI: [10.1016/j.lwt.2007.10.020](https://doi.org/10.1016/j.lwt.2007.10.020).
- [19] Inazu, T.; Iwasaki, K.-i.; Furuta, T. Effect of Temperature and Relative Humidity on Drying Kinetics of Fresh Japanese Noodle (Udon). *LWT* **2002**, *35*, 649–655. DOI: [10.1006/fstl.2002.0921](https://doi.org/10.1006/fstl.2002.0921).
- [20] Crank, J. *The Mathematics of Diffusion*. Oxford: Clarendon Press; **1975**.
- [21] Chen, C. C.; Morey, R. V. Comparison of Four EMC/ERH Equations. *Trans. ASAE* **1989**, *32*, 3, 983–990.
- [22] Dervede, M.; Peglow, M.; Tsotsas, E. Stochastic Modeling of Fluidized Bed Agglomeration: Determination of Particle Moisture Content. *Drying Technol.* **2013**, *31*, 1764–1771. DOI: [10.1080/07373937.2013.810638](https://doi.org/10.1080/07373937.2013.810638).